American Mineralogist, Volume 102, pages 537–547, 2017

SPECIAL COLLECTION: WATER IN NOMINALLY HYDROUS AND ANHYDROUS MINERALS

New SIMS reference materials for measuring water in upper mantle minerals

Kathryn M. Kumamoto[1,*], Jessica M. Warren[2], and Erik H. Hauri[3]

[1]Department of Geological Sciences, Stanford University, 450 Serra Mall, Building 320, Stanford, California 94305, U.S.A.
[2]Department of Geological Sciences, University of Delaware, Penny Hall, 255 Academy Street, Newark, Delaware 19716, U.S.A.
[3]Department of Terrestrial Magnetism, Carnegie Institution of Washington, 5241 Broad Branch Road NW, Washington, D.C. 20015, U.S.A.

Abstract

Trace amounts of water in the nominally anhydrous minerals of the upper mantle can dramatically affect their thermodynamic and rheological properties. Secondary ion mass spectrometry (SIMS) has become a mainstream technique for quantifying small amounts of water in these minerals, but depends on standards with known concentrations of water. The current standards in use for mantle minerals are well-characterized (Hauri et al. 2002; Koga et al. 2003; Aubaud et al. 2007; Mosenfelder and Rossman 2013a, 2013b), but a lack of extra material has limited the spread of this technique to other laboratories.

We present new SIMS measurements on natural mantle xenolith pyroxenes that are suitable for use as calibration reference materials. They are calibrated off of the pyroxene standards currently in use at the Department of Terrestrial Magnetism of the Carnegie Institution of Washington (Koga et al. 2003; Aubaud et al. 2007). They have homogeneous water contents, defined as a standard deviation of <10% for analyses across multiple grains. Reference materials for H_2O cover ranges from 52 to 328 ppm and from 9 to 559 ppm in orthopyroxene and clinopyroxene, respectively, covering most of the observed range of mantle water contents. The samples are evenly distributed over those ranges. The orthopyroxene reference materials can also be used to measure water in olivine based on previous observations that these two minerals have similar calibration slopes.

The new pyroxene reference materials can also be used to calibrate fluorine and phosphorus at low concentrations. We found that fluorine in particular was homogeneous in both orthopyroxene and clinopyroxene, with concentrations of 3 to 50 ppm in orthopyroxene and 0.5 to 118 ppm in clinopyroxene. Phosphorus ranges from below detection up to 19 ppm in orthopyroxene and up to 73 ppm in clinopyroxene, but was more heterogeneous within some samples. Most of the reference materials have concentrations at the lower end of the ranges for fluorine and phosphorus in this study, with only a few samples showing higher concentrations.

Keywords: SIMS, calibration, water, volatiles, nominally anhydrous minerals

Introduction

The upper mantle is largely composed of the nominally anhydrous minerals (NAMs) olivine, orthopyroxene, and clinopyroxene. Water can occur as a trace element in these minerals, dissolved as hydroxyl groups bonded in the crystal structure (e.g., Smyth et al. 1991; Wright and Catlow 1994; Bell et al. 1995; Stalder et al. 2005). The presence of small amounts of water in NAMs influences both physical and chemical properties, including viscosity (e.g., Mackwell et al. 1985; Karato et al. 1986; Hirth and Kohlstedt 1996; Mei and Kohlstedt 2000), melting temperature (e.g., Kushiro et al. 1968), electrical conductivity (e.g., Karato 1990; Schlechter et al. 2012; Sarafian et al. 2015), and seismic wave velocity (e.g., Katayama et al. 2004). The amount of water present in the mantle is poorly constrained, with estimates for total water stored in the mantle varying from 0.25 to 4 times the mass of water in all the Earth's oceans (Hirschmann 2006). Studies have also shown that water distribution is heterogeneous throughout the mantle (e.g., Peslier 2010; Warren and Hauri 2014). To quantify and study the effects of variable amounts of water on mantle properties, techniques are needed to measure very small concentrations of volatiles in NAMs.

Fourier transform infrared spectroscopy (FTIR) has been the most common method used to measure water in NAMs (e.g., Peslier 2010). This technique is ideal for determining site occupancy and can be used to derive absolute concentration as well. However, sample preparation is arduous as it requires doubly polished, oriented grains (e.g., Libowitzky and Rossman 1996; Bell et al. 2003). In addition, subtracting the background signal from this spectroscopic technique can be time consuming and difficult to quantify and reproduce. For example, iron-bearing orthopyroxene and clinopyroxene both have very complex curved baselines (e.g., Goldman and Rossman 1976; Bell et al. 1995; Mosenfelder and Rossman 2013a, 2013b). Calibration of FTIR spectra is also subject to uncertainty, including which peaks should be used to calculate concentration, whether or not the spectra should be polarized, and whether a mineral-specific or frequency-dependent calibration is most appropriate (e.g., Libowitzky and Rossman 1997; Withers et al. 2012; Mosenfelder and Rossman 2013a, 2013b). In particular, the calibration for

* E-mail: kkumamot@stanford.edu
Open access: Article available to all readers online. Special collection information can be found at http://www.minsocam.org/MSA/AmMin/special-collections.html

olivine, the most common mineral in the upper mantle of the Earth, is the subject of considerable debate (e.g., Bell et al. 2003; Aubaud et al. 2009; Kovács et al. 2010; Mosenfelder et al. 2011; Withers et al. 2012).

Over the last 15 years, secondary ion mass spectrometry (SIMS) has become a mainstream technique for measuring water in NAMs (e.g., Koga et al. 2003; Hauri et al. 2006; Aubaud et al. 2007; Ludwig and Stalder 2007; Mosenfelder et al. 2011; Stalder et al. 2012; Withers et al. 2012; Mosenfelder and Rossman 2013a, 2013b). SIMS requires only a single polished surface on an unoriented grain to measure water concentration, making the sample preparation far easier. Traditionally, SIMS has had a relatively high detection limit for hydrogen, making analysis of water in NAMs difficult. Improvements in sample preparation and analytical conditions, however, mean that detection limits can now be as low as a few parts per million H_2O (e.g., Le Voyer et al. 2015).

As a mass spectrometry technique, SIMS necessarily depends on standards with predetermined water concentrations to accurately measure absolute concentrations of water in unknowns. Standards must be matrix-matched since the structure and chemistry of the substrate can have large effects on how easily different elements are ionized by the primary beam of the ion probe (e.g., Deline et al. 1978; Hauri et al. 2002). The standards in use today for olivine, orthopyroxene, and clinopyroxene (e.g., Koga et al. 2003; Aubaud et al. 2007, 2009; Mosenfelder et al. 2011; Mosenfelder and Rossman 2013a, 2013b; Turner et al. 2015) are well characterized but generally limited in supply, making it difficult for this technique to become more widespread. Standards and analytical protocols also vary between laboratories, potentially leading to difficulties in comparing results.

Here, we present measurements on minerals from natural samples (predominantly peridotite xenolith samples that are large in size) that are suitable as SIMS reference materials for the measurement of water in upper mantle minerals. We also present measurements on fluorine and phosphorus in these minerals. Finally, we present details of the data collection and processing steps, including a drift correction technique, to establish a standard analytical protocol.

Sample selection

Samples were chosen from a suite of 34 samples representing various ultramafic sources, including peridotite massifs, pyroxene megacrysts, and peridotite xenoliths. Twenty-three samples were loaned from the Department of Mineral Sciences, Smithsonian Institution, of which 13 were selected as reference materials (their Smithsonian ID is included in Table 1). Nine of these 13 samples were previously described for both water content and major element compositions (Luhr and Aranda-Gomez 1997; Peslier et al. 2002). Three samples from Simcoe were leant by Anne Peslier and Alan Brandon and have also been previously characterized for water content and major elements (Brandon and Draper 1996; Peslier et al. 2002). Two samples from Kilbourne Hole were donated by Jason Harvey, with major and trace elements presented in Harvey et al. (2012). A peridotite xenolith from San Carlos, Arizona, was from the collection of J.M. Warren and has not been previously characterized. Three previously uncharacterized pyroxenes were obtained from the Stanford Mineral Collection, and two were selected as reference materials. In addition, three megacrysts gathered from the Trinity and Josephine Ophiolites were analyzed but proved too altered for use as reference materials.

In total, 15 orthopyroxene and 12 clinopyroxene reference materials were chosen based on high sample abundance, minimal levels of alteration, and homogeneity in pyroxene water content. Table 1 provides a summary of sample mineralogies and localities. For samples where pyroxene chemistry had not been analyzed, we used the JEOL JXA-8230 Electron Microprobe at Stanford University to measure the abundances of major elements Si, Al, Ti, Cr, Mn, Mg, Ca, Fe, Na, and Ni. Current was maintained at 30 nA using a 15 kV beam and an 8 μm spot size. Ten adjacent analyses were gathered perpendicular to any apparent exsolution lamellae on each grain to constrain sample chemistry.

All pyroxenes are plotted in Figure 1 on a pyroxene Mg-Ca-Fe ternary, and a compilation of their major element chemistry is provided in Supplemental[1] Table 1. For all samples presented here, orthopyroxene compositions correspond to predominantly enstatite with small amounts of iron and calcium. Al_2O_3 concentrations range from 1.9 to 5.6 wt%. Clinopyroxene compositions are generally chrome diopside with some variation in the amount of calcium incorporated. Aluminum contents cover a larger range for clinopyroxene than orthopyroxene, varying between 0.1 and 7.7 wt%. These compositions fall within the range of typical mantle pyroxenes (gray background points in Fig. 1), with the exception of one diopside, SMC31139. This mineral specimen is from a nickel mine bordering a hydrothermally altered serpentinite (see Tarassoff and Gault 1994, for a summary of the geology of the mine) and is a 4:1 diopside:hedenbergite solid solution (Fig. 1).

Secondary ion mass spectrometry

Sample preparation

To prepare mounts for SIMS analyses, xenoliths and megacrysts were lightly crushed, and grains of each mineral phase were picked based on optical purity. Grains were cleaned by sonicating in DI water for 1 min before rinsing in ethanol and drying overnight. To create a mount, grains were pressed into indium-filled 1-inch aluminum rounds (e.g., Koga et al. 2003; Aubaud et al. 2007). A grain of Suprasil 3002 glass (1 ppm H_2O certified by Heraeus Quarzglas) or synthetic forsterite (0.04 ppm H_2O, Koga et al. 2003) was included in each mount for measuring the background water content of the instrument. Suprasil glass in particular had reproducible low water concentrations, making it the recommended material for use as a blank. A grain of ALV-519-4-1 basaltic glass was also always included to track instrumental drift over the course of a session. Mounts were ground by hand with SiC sandpaper to expose the approximate center of each grain. They were then polished using diamond solutions down to a 1 μm polish before being cleaned again with DI water and ethanol.

Analytical conditions

Water concentrations in NAMs were measured in mineral grains using the Cameca IMS 6f ion microprobe at the Department of Terrestrial Magnetism (DTM), Carnegie Institution of Washington. Data for this study were gathered over three analytical sessions in July 2014, April 2015, and January 2016. Prior to analysis, mounts were stored in a vacuum oven at 50 °C for at least 12 h, then removed and coated with ~40 nm of gold. Samples were introduced into the exchange chamber at least 24 h before being moved into the main chamber to maintain the

[1]Deposit item AM-17-35863, Supplemental Figures and Tables. Deposit items are free to all readers and found on the MSA web site, via the specific issue's Table of Contents (go to http://www.minsocam.org/MSA/AmMin/TOC/2017/Mar2017_data/Mar2017_data.html).

TABLE 1. Description of samples

Sample	SMNH ID	Locality	Lithology	Selected minerals	References
	109426-1	Salt Lake Craters, Hawaii	Lherzolite xenolith	Opx	
BCN-200	116610-26	San Quintin Volcanic Field, Mexico	Lherzolite xenolith	Opx	1, 2
BCN-203	116610-29	San Quintin Volcanic Field, Mexico	Lherzolite xenolith	Opx	1, 2
DGO-160	116610-18	Durango Volcanic Field, Mexico	Lherzolite xenolith	Cpx, Opx	1, 2
DGO-166	116610-21	Durango Volcanic Field, Mexico	Lherzolite xenolith	Cpx, Opx	1, 2
KH03-4		Kilbourne Hole, New Mexico	Lherzolite xenolith	Cpx, Opx	3
KH03-27		Kilbourne Hole, New Mexico	Lherzolite xenolith	Cpx, Opx	3
PR-7-2	117322-242	Premier Kimberlite, Transvaal, Africa	Kimberlite chrome diopside megacryst	Cpx	
PR-7-5	117322-245	Premier Kimberlite, Transvaal, Africa	Kimberlite enstatite megacryst	Opx	
SC-J1		San Carlos, Arizona	Lherzolite xenolith	Cpx	
Sim-9c		Simcoe Volcano, Washington	Lherzolite xenolith	Opx	1, 4
Sim-24		Simcoe Volcano, Washington	Lherzolite xenolith	Opx	1, 4
SLP-101	116610-14	Ventura Volcanic Field, Mexico	Lherzolite xenolith	Cpx	1, 2
SLP-108	117213-5	Ventura Volcanic Field, Mexico	Clinopyroxenite in lherzolite xenolith	Cpx, Opx	
SLP-114	116610-10	Ventura Volcanic Field, Mexico	Harzburgite xenolith	Opx	1, 2
SLP-142	116610-5	Santa Domingo Volcanic Field, Mexico	Lherzolite xenolith	Cpx, Opx	1, 2
SLP-402	116610-15	San Quintin Volcanic Field, Mexico	Lherzolite xenolith	Cpx, Opx	1, 2
SLP-403	116610-16	San Quintin Volcanic Field, Mexico	Lherzolite xenolith	Cpx, Cpx	1, 2
SMC31139		Orford Nickel Mine, Quebec , Canada	Diopside	Cpx	

Note: Previous work on both major element chemistry and water content is included in the reference column. Samples with Smithsonian (SMNH) ID numbers were provided by the Department of Mineral Sciences, Smithsonian Institution. References: [1] Peslier et al. (2002), [2] Luhr and Aranda-Gomez (1997), [3] Harvey et al. (2012), [4] Brandon and Draper (1996).

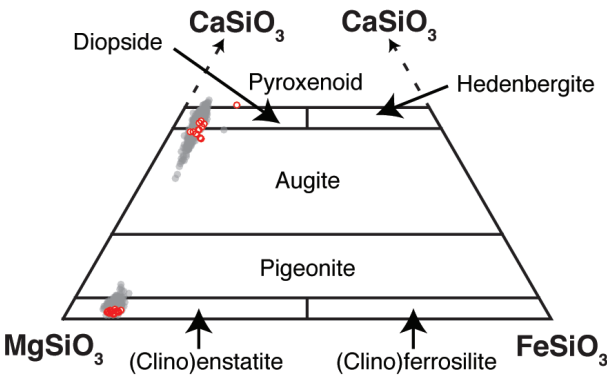

FIGURE 1. Depiction of pyroxene major element compositions on the pyroxene quadrilateral. Orthopyroxenes fall in the bottom left corner, near enstatite, while clinopyroxenes cluster near the upper left, near diopside. Data from this study are shown as red circles. The gray data points of the background field are from the Warren (2016) abyssal peridotite database.

ultrahigh vacuum ($P < 10^{-9}$ torr) necessary for measuring volatiles in nominally anhydrous minerals.

Analyses were made using a rastered Cs^+ beam with a current of 15–25 nA and an accelerating voltage of 10 kV. Charge compensation was provided by an electron flood gun. The sputter pits typically measure ~30–40 μm in diameter, but counts were only collected from the center 10 μm of each pit by using the smallest field aperture. After five minutes of presputtering, the magnet was cycled through masses ^{12}C, $^{16}O^1H$, ^{19}F, ^{30}Si, ^{31}P, ^{32}S, and ^{35}Cl. Counting times were 10 s for ^{12}C and 5 s for all other masses. Five cycles of data were collected per analysis using the electron multiplier, and a deadtime correction was automatically applied. The blank (Suprasil 3002 glass or synthetic forsterite) and secondary standard (ALV-519-4-1) were measured every 10–20 analyses.

Calibration

Standards from Hauri et al. (2002), Koga et al. (2003), and Aubaud et al. (2007) were run at the beginning of each analytical session. The basaltic glass standards ALV-519-4-1, WOK-28-3, ALV-1654-3, ALV-1833-1, ALV-1833-11, and ALV-1846-12, calibrated by Hauri et al. (2002), were run first. Volatile concentrations and silica contents for these glasses are listed in Table 2. Since these glasses contain higher concentrations of water than the NAM standards, they are generally easier to measure and a good first estimate of machine conditions.

Standards used for measuring water in orthopyroxene were Opx A288, India Enstatite, KBH-1, and ROM-273-OG2. Clinopyroxene standards were

TABLE 2. Composition of DTM basaltic glass standards

Sample	SiO_2 (wt%)	H_2O (ppm)	F (ppm)	P (ppm)	References
ALV-519-4-1	49.07	1700 (43)	95	302	1, 2
WOK-28-3	49.77	4900 (245)	185	545	1, 3, 5
ALV-1654-3	56.67	10000 (500)	975	2840	
ALV-1833-11	51.13	11700 (585)	195	786	1, 3, 4, 5
ALV-1846-12	50.75	15800 (790)	288	786	1, 3, 4, 5
ALV-1833-1	50.33	19800 (990)	446	1095	1, 3, 4

Notes: Concentrations of SiO_2 in weight percent. Concentrations of volatiles in parts per million by weight. 1σ uncertainties for water concentrations in parts per million by weight. References: [1] Hauri et al. (2002), [2] Bryan and Moore (1977), [3] Stolper and Newman (1994), [4] Volpe et al. (1990), [5] Hawkins et al. (1990).

ROM-271-10, PMR-53, ROM-271-16, and ROM-271-21. Compositions and references for these standards are in Table 3. Most of these standards have been calibrated with FTIR (Koga et al. 2003; Aubaud et al. 2007). Importantly, however, the orthopyroxene KBH-1 and the clinopyroxene PMR-53 were measured by vacuum manometry by Bell et al. (1995) and thus provide calibration anchor points that are independent of FTIR integration methods and choice of absorption coefficients. PMR-53 is known to fall off the calibration curve for clinopyroxene (possible reasons are discussed in Mosenfelder and Rossman 2013b), but until more absolute measurements of water in clinopyroxene are made, this remains an unresolved issue.

Calibration curves were constructed using a weighted least-squares linear regression of water content vs. the $^{16}O^1H/^{30}Si$ counts ratio and forced through the origin. The regression was done in MATLAB using the function *lscov* with a weight assigned to each point. Weighting was based on the uncertainty in the accepted FTIR or manometry values for water content. The uncertainty in the $^{16}O^1H/^{30}Si$ count ratio was excluded because it was much smaller than the uncertainty in the accepted values. The 1σ standard error on the calibration slope was typically around 4% for orthopyroxene and around 12% for clinopyroxene. The higher error in the slope for the clinopyroxene calibration was due to the relatively wide spread of standards around the calibration line, a consistent characteristic of these standards also observed by Mosenfelder and Rossman (2013b).

Water contents of one of the orthopyroxene standards (India Enstatite) and three of the clinopyroxene standards (PMR-53, ROM-271-16, and ROM-271-21) were analyzed by Aubaud et al. (2009) using three different FTIR calibrations (Paterson 1982; Bell et al. 1995; Libowitzky and Rossman 1997), as well as by elastic recoil detection analysis (ERDA). Since India Enstatite is the only common orthopyroxene standard between Aubaud et al. (2009) and the DTM standards used in this study, we have used the values for this standard from Koga et al. (2003), which is based on the Bell et al. (1995) FTIR calibration for orthopyroxene (Table 3). For clinopyroxene, the results of the Aubaud et al. (2009) analyses differ dramatically from each other depending on the FTIR calibration and the technique, similar to the results of Mosenfelder and Rossman (2013b) on an overlapping set of standards. These differences have large effects on the calculated calibration slope, and thus the calculated water contents of new samples. We have chosen to continue using

TABLE 3. Water concentrations in DTM pyroxene standards

Sample	Mineral	H_2O (ppm)	References
A288	Opx	44 (8)	1
India Enstatite	Opx	141 (7)	1, 2
KBH-1	Opx	217 (11)	1, 2, 3
ROM-273-OG2	Opx	263 (13)	2, 4
ROM-271-DI10	Cpx	195 (10)	2, 4
PMR-53	Cpx	268 (14)	1, 2, 3
ROM-271-DI16	Cpx	439 (22)	2, 4
ROM-271-DI21	Cpx	490 (25)	2, 4

Notes: Concentrations and 1σ uncertainties in parts per million by weight. References: [1] Koga et al. (2003), [2] Aubaud et al. (2007), [3] Bell et al. (1995), [4] Bell et al. (2004).

values calculated by Koga et al. (2003) and Aubaud et al. (2007) based on the Bell et al. (1995) FTIR calibration (Table 3). This allows for direct comparisons to be made with many FTIR data sets for water in diopsides and calcium-rich augites, which mainly use the Bell calibration (e.g., Grant et al. 2007; Bonadiman et al. 2009; Xia et al. 2010; Doucet et al. 2014; Peslier and Bizimis 2015). Published SIMS data sets also often use standards based on the Bell et al. (1995) calibration to measure water in pyroxenes (e.g., Warren and Hauri 2014).

Since matrix-matched standards do not yet exist for other volatiles in mantle minerals, we used the basaltic glass standards run at the beginning of each session to quantify the concentrations of fluorine and phosphorus (Table 2). As with the water calibrations, these data were fit with a weighted least-squares linear regression to create the fluorine and phosphorus calibrations.

Data processing

To process the SIMS data, the following steps were completed: (1) removal of bad data cycles and ratioing of volatile counts to ^{30}Si counts, (2) background correction, (3) instrumental drift correction by analysis number and by mount, (4) filtering of data for statistical anomalies and contamination, and finally, (5) application of the calibration curve to calculate final concentrations.

Volatile counts were initially ratioed to ^{30}Si as a first step to average out the effects of instrument drift. Fluctuations in primary ion beam current during a single analysis can result in changes in count magnitude for all species measured. By ratioing to ^{30}Si, the effects of such fluctuations are mitigated. Bad data cycles, the result of an electronic glitch in the DTM 6f SIMS, were identified as a drop to near zero counts for one mass in a single cycle. These cycles were removed.

Synthetic forsterite or Suprasil 3002 glass (depending on the mount) was used to measure the background volatile content of the instrument. These grains were measured regularly during each session, and the average background count ratios for a mount were calculated. The ratios $^{16}OH^1/^{30}Si$, $^{19}F/^{30}Si$, and $^{31}P/^{30}Si$ were then used to correct for background water, fluorine, and phosphorus by subtracting the mount average background from each individual unknown measurement on the mount.

We used analyses of basaltic glass ALV-519-4-1 as a secondary standard to further account for instrumental drift as well as changes in instrumental conditions between mounts. This secondary standard has proven to be a very reproducible, homogeneous standard for all elements measured under the above analytical conditions. Le Voyer et al. (2015) report a standard deviation <2.5% for all volatiles in ALV-519-4-1 for >250 analyses collected over two years. If instrument conditions do not change over the course of an analytical session, ALV-519-4-1 analyses should always have the same count ratios throughout the session. Since instrument conditions do change, for instance due to putting in a new mount or refocusing the primary beam, the secondary standard is used to correct for instrumental drift among analyses in a single mount, as well as differences between mounts (K-factor correction). Mathematical details of the two ALV-519-4-1 corrections are provided in the appendix[1].

Instrumental drift between analyses on an individual mount was identified as linear trends in volatile count ratios in the glass against analysis number, which is a proxy for time. This drift was removed using a percentage correction function and was applied to every analysis, including analyses of ALV-519-4-1. The correction nearly always recovers values for ALV-519-4-1 that are within 10% of the average count ratio for analyses of ALV-519-4-1 on a given mount. A new correction function was used for each indium mount, and a new correction function was usually calculated every day for mounts that ran over multiple days.

The K-factor correction was then applied after the drift correction to account for differences in count ratios between mounts, which are ultimately due to changes in instrument conditions when the mount is changed. This was done by calculating the percent change required to bring the ALV-519-4-1 analyses on the unknown mount into agreement with the ALV-519-4-1 analyses on the standard mount (upon which the calibration is based) and applying that percentage change to all analyses on the unknown mount. This correction makes the average $^{16}O^1H/^{30}Si$ ratio of ALV-519-4-1 for each new mount equal the value for ALV-519-4-1 run during the standard calibration.

Standard analyses during one session—conducted in April 2015—resulted in calculated values for H_2O in ALV-519-4-1 that were anomalously high by 5.3 rel% compared with other analytical sessions before and afterward. As a result, the K-factor correction for all analyses in the April 2015 session was reduced by 5.3% to bring the calculated H_2O values for ALV-519-4-1 into consistency with other analytical sessions.

The ratios $^{12}C/^{30}Si$, $^{32}S/^{30}Si$, and $^{35}Cl/^{30}Si$ were used to monitor for compromised analyses. High counts in any of these elemental ratios are assumed to indicate interference from surface contamination, inclusions, fracture material, or alteration, and these analyses were discarded. Points with variable $^{16}O^1H/^{30}Si$ count ratios (>1.5% error as measured over 5 cycles) were also removed from the final data set. Data reduced to this point are reported in Supplement[1] 3.

In the final step of data processing, the calibrations were applied to the remaining analyses to calculate the concentrations of volatiles in the unknowns. For all samples, this was done by multiplying the corrected volatile count ratios by the slope of the appropriate calibration line. Calibration data for each session are reported in Supplement[1] 3.

RESULTS

The results of our SIMS analyses are presented in Table 4. The data are plotted in Figures 2 and 3 as box-and-whisker plots of all good analyses across all grains on a sample-by-sample basis. In these plots, the boxes contain 50% of the analyses centered around the median, while the whiskers show the range of all analyses. Some samples show larger variability in water content than others, but all fall under the 10% standard deviation cut-off imposed as a measure of homogeneity.

Water contents in orthopyroxene range from 52 to 328 ppm, while the range in clinopyroxene is from 9 to 559 ppm. Reference materials are relatively evenly distributed across the range in water contents for each phase (Fig. 2). Fluorine varies between 3.0 and 50.3 ppm in orthopyroxene and between 0.5 and 118.2 in clinopyroxene, while phosphorus concentrations range from below detection to 18.6 ppm in orthopyroxene and to 72.8 ppm in clinopyroxene (Fig. 3). Water does not exhibit any covariation with either of these two elements. Concentrations are generally homogeneous for both elements, but a few samples show large compositional variations in phosphorus while maintaining homogeneity in water and fluorine.

Table 4 presents error calculated in two ways: (1) the standard deviation of repeat analyses on grains from the same sample, and (2) the propagated uncertainties of the final values, taking into account the uncertainty in the blank measurement and the uncertainty on the slope of the DTM calibration line. The first error estimate, based on repeat analyses of a sample, provides the best representation of reproducibility. This estimate was used to determine the homogeneity of each sample. As the goal of this study is to create new reference materials for SIMS analyses of water concentration in NAMs, samples were only selected as reference materials, and thus reported here, if they are homogeneous with respect to water, with a standard deviation of less than 10% among analyses on multiple grains. A minimum of 10 analyses over at least 2 grains was required for this criteria, with up to 134 analyses over 8 grains for an individual sample (KH03-27 orthopyroxene) in this study. The second method for estimating error provides a more accurate representation of

TABLE 4. Volatile concentrations in pyroxene reference materials

Sample	No. of Grains	No. of Analyses (% good)	Water			Fluorine			Phosphorus		
			Conc. (ppm)	St.Dev. (ppm)	Prop. 1σ (ppm)	Conc. (ppm)	St.Dev. (ppm)	Prop. 1σ (ppm)	Conc. (ppm)	St.Dev. (ppm)	Prop. 1σ (ppm)
Orthopyroxene											
116610-29	2	25 (92%)	62	4	5	15.1	0.6	0.8	1.1	0.2	0.2
Sim-9c	2	17 (100%)	82	6	7	11.4	0.6	0.7	1.6	2.2	2.2
Sim-24	2	13 (87%)	110	7	8	14.8	0.4	0.7	b.d.		
116610-18	4	29 (91%)	119	10	11	22.7	1.1	1.4	1.3	0.2	0.2
116610-10	5	47 (100%)	128	12	12	17.4	1.0	1.2	0.5	0.1	0.1
117213-5	2	19 (95%)	169	9	11	4.5	0.2	0.3	3.3	0.3	0.3
KH03-27	9	104 (80%)	182	18	19	14.8	0.7	0.9	1.5	0.3	0.3
117322-245	2	14 (88%)	211	10	12	27.4	0.9	1.4	4.3	0.2	0.3
116610-21	2	26 (87%)	215	20	21	9.0	0.4	0.5	5.0	0.5	0.6
KH03-4	6	48 (96%)	216	12	14	25.0	0.9	1.3	10.6	0.8	0.9
116610-15	6	48 (91%)	234	21	22	50.3	2.2	2.9	10.0	1.6	1.7
116610-26	2	20 (100%)	237	19	20	9.1	0.6	0.7	2.5	0.5	0.5
109426-1	2	16 (84%)	241	14	15	22.0	0.9	1.2	18.6	11.2	10.9
116610-16	5	41 (95%)	264	26	28	23.6	1.1	1.4	6.7	1.0	1.0
116610-5	2	16 (89%)	309	26	27	3	0.2	0.2	1.8	0.2	0.2
Clinopyroxene											
SMC31139	4	30 (80%)	5	8	8	0.5	0.3	0.3	b.d		
SC-J1	6	43 (93%)	62	4	9	26.0	1.2	1.6	30.9	14.6	14.5
117322-242	6	25 (63%)	127	5	16	69.5	1.8	3.3	13.0	1.1	1.3
116610-18	5	29 (88%)	199	13	27	54.0	2.0	3.0	3.6	0.8	0.8
117213-5	4	28 (90%)	315	15	40	13.0	1.7	1.7	11.1	0.6	0.8
116610-21	2	16 (94%)	354	28	50	23.5	1.1	1.4	15.5	1.3	1.5
116610-14	4	19 (83%)	356	22	48	57.8	1.0	2.5	72.8	14.0	14.2
KH03-27	7	46 (96%)	367	18	49	39.4	1.5	2.2	5.3	0.5	0.6
116610-15	4	21 (100%)	441	31	61	118.2	1.8	5.0	46.6	1.7	3.1
KH03-4	4	26 (96%)	427	25	59	64.8	2.2	3.3	38.0	1.0	2.3
116610-16	2	19 (95%)	490	33	66	58.8	2.4	3.2	29.5	3.0	3.3
116610-5	2	8 (80%)	544	49	79	7.8	0.2	0.4	7.8	0.2	0.5

Notes: All concentrations and uncertainties given in parts per million by weight. The two uncertainties given for each volatile are described in the text. The number of analyses presented in this table represents the number of analyses that passed all data reduction tests. The percent of analyses that passed the data reduction tests is also presented in the same column.

the uncertainty in absolute concentration as it accounts for the uncertainties in the DTM calibration.

Table 4 also reports the number of analyses that passed all data reduction tests and thus contribute to the final values for each volatile. The percentage of total analyses represented by this subset is also reported. The discarded analyses are ones that were classified as compromised due to high counts of C, S or Cl, or variable OH ratios during analysis. Based on petrographic examination, a small number of samples contain fluid inclusions, mainly concentrated along microcracks (Fig. 4) and possibly following specific crystallographic planes. Inclusions are not present in all grains, however, and all of the crystals we examined have large clean areas with no inclusions. If the primary ion beam hits an inclusion, either solid or fluid, fluctuations occur in water content over the course of the five data cycles and/or detectable amounts of carbon, sulfur, or chlorine are found. These types of analyses are removed by the data reduction routine.

For example, sample 117322-242 contains small inclusions that can be seen with scanning electron microscopy. The comparatively low percentage of good analyses (62.5%) for this diopside megacryst is indicative of the high number of inclusions in this sample. However, the narrow spread of water content over the 25 good analyses of 117322-242 (4% 1σ standard deviation) is also indicative of a high degree of sample homogeneity away from the inclusions and that our data processing easily removes bad analyses. We expect that alteration (e.g., serpentine or amphibole) would be similarly simple to detect, though the samples presented in this study show little evidence for any pervasive alteration.

DISCUSSION

Calibration reference materials for water

We have created a new set of pyroxene calibration reference materials for SIMS measurements of volatiles in mantle NAMs (Table 4, Figs. 2 and 3). These reference materials are suitable for the calibration of water in olivine as well as pyroxene, as olivine has the same calibration slope as orthopyroxene (Koga et al. 2003; Kovács et al. 2010; Withers et al. 2011; Mosenfelder and Rossman 2013a; Warren and Hauri 2014). For each sample, we have characterized several grains of each phase and used this to select reference materials that have homogeneous water contents within 10% standard deviation and no detectable diffusional gradients outside of error. Occasionally in these grains, an individual analysis may appear anomalously high or low compared to other repeat analyses, despite looking like a good analysis according to the data reduction process. For calibration purposes, if an individual analysis falls far away from other repeat analyses, it should be removed from the calibration curve.

While our standard deviation values (Table 4) are larger than those of current standards (Koga et al. 2003; Aubaud et al. 2007; Mosenfelder and Rossman 2013a, 2013b), our samples have a larger number of repeat measurements over multiple grains and multiple sessions. The opportunity to collect so many data points allows us to better estimate the uncertainty in concentrations.

Data are also presented on a grain-by-grain basis in Supplemental[1] Figure 1 and Supplemental[1] Table 2. In general, averages by grain have lower standard deviations than the averages by sample, most likely due to all points on a grain being measured

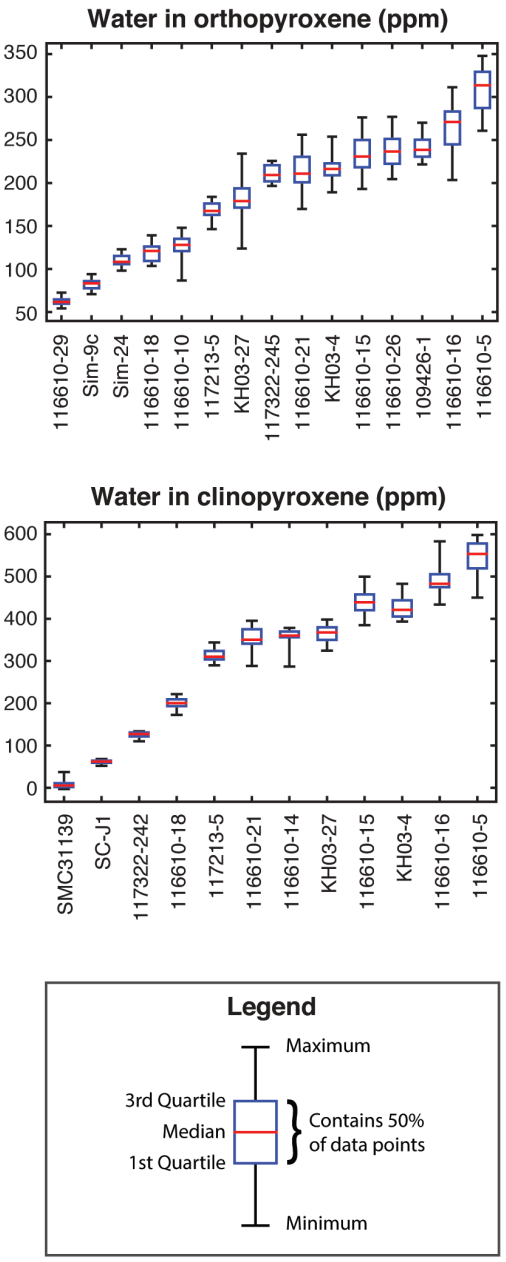

Figure 2. Water measurements in pyroxene reference materials displayed as box-and-whisker plots of all analyses within a sample that were not removed by the data reduction process. The median of the data is displayed as a red line, and the first and third quartiles define the edges of the box. The whiskers extend to the maximum and minimum analyses to show the full range of water concentrations measured for each sample.

consecutively within a short time period during a session. Any instrumental drift during this time should be negligible, whereas changes in conditions between grains on the same mount, on different mounts, and during different sessions could be far larger. The observed intergranular variations may also be due to real variations in water content, and the potential always exists that other grains may show resolvable zonation within the sample. Therefore, when using these samples as reference materials, we recommend using the sample averages and propagated uncertainties for calculating calibration curves, as these values account for more possible sources of uncertainty and better represent the intra- and inter-session behavior of these materials.

To confirm the validity of our new reference material set, a subset of the orthopyroxene samples were run in conjunction with the DTM standards on the Stanford University Cameca NanoSIMS 50L using a 10 nA Cs^+ beam and an accelerating voltage of 8 kV. After a 3 min presputter on a 30 × 30 μm area, analyses were collected on a centered 10 × 10 μm raster with electronic gating to the central 3 × 3 μm area. Masses were collected simultaneously using a multi-collector, with 5 blocks of 10 frames each gathered in 50 s. After a correction using ALV-519-4-1 to bring count ratios across the mounts into alignment, the two sets of calibration materials produced nearly identical calibration curves (Fig. 5).

Our reference materials are unusual in that we are using water concentrations determined by SIMS to create new reference materials for SIMS. The absolute concentration of water in calibration standards are more typically measured using alternative techniques, such as FTIR, ERDA, nuclear reaction analysis (NRA), or hydrogen manometry (e.g., Koga et al. 2003; Aubaud et al. 2007; Mosenfelder et al. 2011; Mosenfelder and Rossman 2013a, 2013b; Turner et al. 2015). However, each of these techniques has its own drawbacks. Hydrogen manometry, for instance, requires a large sample of clean material that is destroyed in the process of making the measurement (e.g., Rossman 2006). ERDA generally has a high background water content, as observed by Aubaud et al. (2009), making measurements of very low water concentrations, such as those present in natural mantle olivine, difficult. NRA can achieve very low detection limits (e.g., Endisch et al. 1994; Bell et al. 2003; Maldener et al. 2003) but is not easily accessible. FTIR, as mentioned earlier, suffers from difficulties in selecting the proper calibration, proper removal of background, and time-intensive sample preparation.

We purposely only calibrated our reference materials against the DTM standards, meaning they are entirely dependent on the values of those standards, which were calibrated by Bell et al. (1995), Hauri et al. (2002), Koga et al. (2003), and Aubaud et al. (2007). This means that any future revisions to the DTM standard values will be straightforward to propagate through our reference material values. The standards in use at DTM (Bell et al. 1995; Hauri et al. 2002; Koga et al. 2003; Aubaud et al. 2007) and Caltech (Mosenfelder et al. 2011; Mosenfelder and Rossman 2013a, 2013b) currently represent the best-constrained set of standards that we are aware of for the analysis of water in olivine and pyroxenes via SIMS. These standards include two grains with manometry measurements of water content by Bell et al. (1995): the orthopyroxene KBH-1 and the clinopyroxene PMR-53. However, most of the DTM standards were calibrated via FTIR and may be subject to future revisions, particularly as more research is done into mineral-specific vs. frequency-dependent calibrations and the background correction. Solving these problems will require more absolute measurements of water (e.g., by ERDA, NRA, or manometry). When this occurs, the water concentrations of the reference materials presented here could be revised by calculating a new calibration curve based on updated values for the original DTM standards. This situation

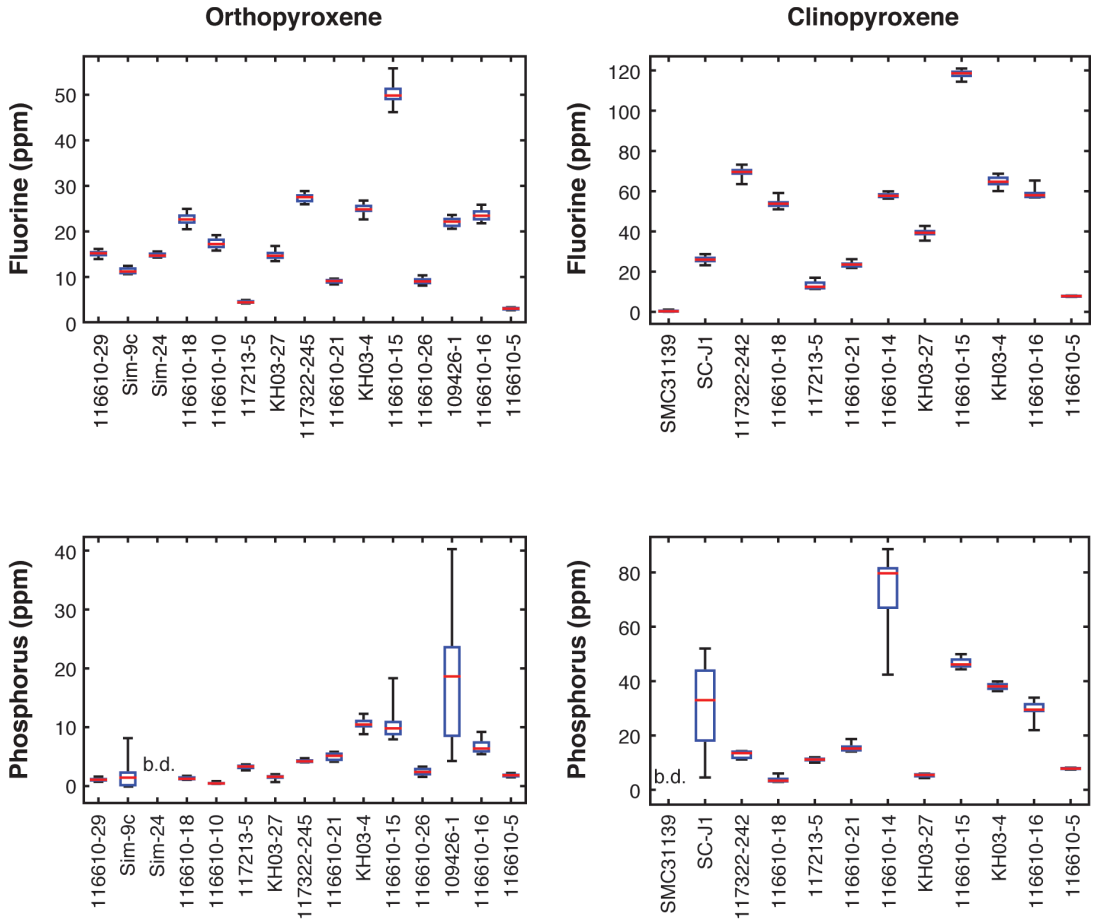

FIGURE 3. Fluorine and phosphorus measurements in pyroxene reference materials displayed as box-and-whisker plots. For an explanation of the plot style, see Figure 2.

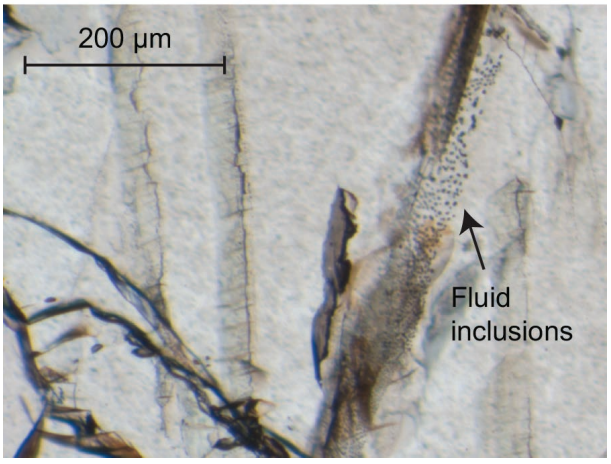

FIGURE 4. Example of fluid inclusions in an orthopyroxene grain in a thin section of 116610-29. Image taken in plane-polarized transmitted light.

would only require re-processing of the final step of the data reduction to apply the updated calibration, and the data necessary for this are provided in Supplemental[1] Table 3. Updating the calibration would result in a shift in the absolute value of samples, but observations of relative variability among samples would remain unchanged. As the accuracy of the calibration curves improves, the error associated with SIMS analyses will be reduced.

A subset of our reference materials have been previously measured by FTIR by Peslier et al. (2002). Our values for this sample subset are offset from those of Peslier et al. (2002), as shown in Figure 6. For clinopyroxene, this offset is fairly minor and randomly distributed about the 1:1 line. In contrast, orthopyroxene shows a systematic offset with almost all SIMS data having higher concentrations than the FTIR data (Fig. 6). As Peslier et al. (2002), Koga et al. (2003), and Aubaud et al. (2007) all use the Bell et al. (1995) mineral-specific calibrations, we attribute the discrepancy between our SIMS values and the Peslier et al. (2002) values to the method of FTIR background removal. In Peslier et al. (2002), the background was determined by experimentally dehydrating a single xenolith sample and using FTIR spectra gathered from this sample as the background for all samples in the study. Each mineral phase in each xenolith has its own baseline, however, due to influences from composition, oxidation state, and precise orientation of the grain. Thus, using dehydration spectra to determine baselines would be better done by dehydrating a grain of each mineral for each

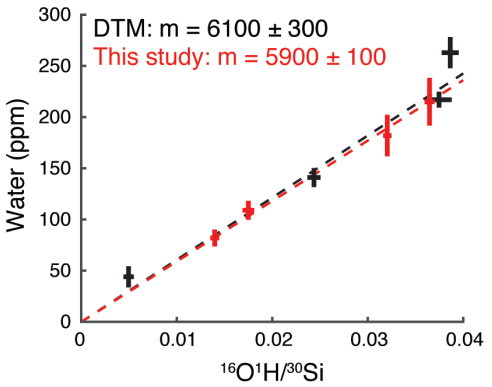

FIGURE 5. Comparison of calibration lines for orthopyroxene produced by the DTM standards (Koga et al. 2003; Aubaud et al. 2007) and the reference materials presented in this study, with concentration on the y-axis in parts per million and the counts ratio $^{16}O^{1}H/^{30}Si$ on the x-axis. Samples were run on the Stanford Cameca NanoSIMS 50L. Error bars are 1σ. For water concentration in the reference materials from this study, the propagated uncertainty (Table 4) is used. Uncertainty in the counts ratios is the standard deviation of 2–3 repeat measurements on the same grain. The calibration lines produced by the two sets of calibration materials fall within error of each other and are in fact nearly coincident.

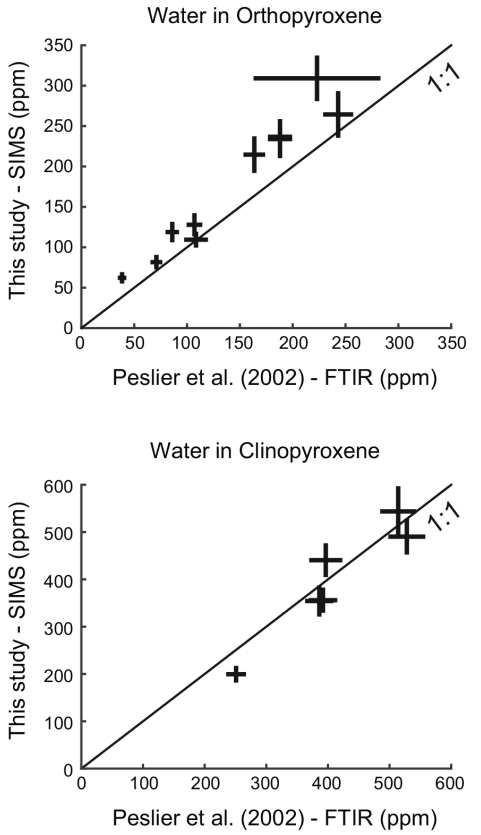

FIGURE 6. Comparison of SIMS data collected by this study and FTIR measurements collected by Peslier et al. (2002). Error bars are 1σ for both SIMS and FTIR, using the propagated uncertainty in Table 4 for the SIMS data. The black line is the 1:1 correspondence line for the two techniques.

sample (Peslier, personal communication). Koga et al. (2003) and Aubaud et al. (2007), on the other hand, both employed a polynomial baseline fit to remove the background of samples in their studies. Given the uncertainty of previous work, future FTIR work on the samples in this study may resolve the offset seen between the FTIR and SIMS measurements.

Fluorine and phosphorus

The fluorine and phosphorus data presented in this study allows these samples to be used as reference materials for low concentrations of these elements. Most of the samples are homogeneous for fluorine (Fig. 3), with a standard deviation ranging from 2 to 7% (1σ) for orthopyroxene and clinopyroxene, except for two low-fluorine orthopyroxenes (Table 4). Phosphorus, on the other hand, is homogeneous in some of our samples, but highly heterogeneous in others (Fig. 3), with the standard deviation for a sample ranging from 2–150% (1σ; Table 4). For both elements in both phases, however, a subset of the reference materials have <10% 1σ standard deviation and can be used to create a calibration curve suitable for low concentrations of fluorine and phosphorus. For higher concentrations, a basaltic glass calibration should be used.

The overall issue with the fluorine and phosphorus calibrations is the lack of independently calibrated pyroxenes, resulting in calibration curves that are not matrix-matched to pyroxenes. We used a set of basaltic glasses to create calibration curves for these elements (Table 2). These glass standards were calibrated off of another set of four glass standards with known fluorine concentrations (Hauri et al. 2002). We chose not to scale our calibrations to the glass silica contents in the manner of Mosenfelder and Rossman (2013a, 2013b), because a scaling correction is not clearly necessary based on the limited data set. The difference in final concentrations of fluorine and phosphorus in the pyroxenes between a calibration scaled with silica content in the glasses and pyroxenes vs. a calibration not scaled with silica is very minor (~2.5%). Once standards have been analyzed for fluorine and phosphorus by an independent method, the calibration procedure here can be updated to incorporate scaling with silica content if appropriate.

Fluorine concentrations in orthopyroxene and clinopyroxene cover a range (Opx = 3–50 ppm; Cpx = 0.5–118 ppm) similar to that seen by Gazel et al. (2012) in mantle xenoliths (Opx = 13–43 ppm; Cpx = 30–111 ppm) and Warren and Hauri (2014) in peridotites from various tectonic settings (Opx = 0.2–26 ppm; Cpx = 0.1–66 ppm). Recent observations of fluorine in mantle xenoliths extend to higher concentrations than those observed here, with values of up to 200 ppm in pyroxenite veins (e.g., Rooks et al. 2015). The range of phosphorus concentrations in abyssal peridotites studied by Warren and Hauri (2014) (Opx = 1–12 ppm; Cpx = 5–32 ppm) is similar to that reported here (Opx = b.d. to 18 ppm; Cpx = b.d. to 73 ppm). However, Brunet and Chazot (2001), Witt-Eickschen and O'Neill (2005), and Mallmann et al. (2009) measured phosphorus concentrations in peridotite xenoliths that are beyond the range represented in our reference materials (combined range of these sources: Opx = 5–40 ppm, Cpx = 9–148 ppm).

As previously mentioned, some of the pyroxenes have very variable phosphorus content. Zoning in phosphorus content is

well known in igneous olivine, which also has an overall higher abundance of phosphorus, and this zoning is often attributed to complex crystallization processes (e.g., Toplis et al. 1994; Milman-Barris et al. 2008; Welsch et al. 2014; Watson et al. 2015). Mallmann et al. (2009) found phosphorus zoning in mantle olivine from Australian xenoliths and suggested that the patterns were due to metasomatism and deformation. Notably, however, Mallmann et al. (2009) saw no apparent zoning of phosphorus in the pyroxenes from those same samples. The variability in the phosphorus data we present here suggests that zoning may be important in some xenoliths and is worth future exploration.

Volatile partitioning

We examined the partitioning behavior of volatiles between orthopyroxene and clinopyroxene in the seven samples where both phases were present, measured, and homogeneous. In Figure 7, volatile concentrations in clinopyroxene are plotted against orthopyroxene and compared to other data sets. For water, our data falls in the same range as that seen in a literature compilation of natural samples (Bell and Rossman 1992; Peslier et al. 2002; Demouchy et al. 2006; Aubaud et al. 2007; Grant et al. 2007; Falus et al. 2008; Li et al. 2008; Yang et al. 2008; Bonadiman et al. 2009; Xia et al. 2010; Yu et al. 2011; Hao et al. 2012; Peslier et al. 2012; Denis et al. 2013; Xia et al. 2013; Hao et al. 2014; Warren and Hauri 2014; Bizimis and Peslier 2015; Hui et al. 2015; Peslier and Bizimis 2015; Hao et al. 2016). The partition coefficient obtained from this literature compilation is 2.4 ± 0.9. The high uncertainty reflects the variety of methods, localities, and degrees of sample dehydration or alteration present in this compilation. Experimental partition coefficients measured by Aubaud et al. (2004), Hauri et al. (2006), Tenner et al. (2009), and Rosenthal et al. (2015) are lower than that observed in natural samples, at $D_{H_2O}^{Cpx/Opx} = 1.3 \pm 0.2$. Potential reasons for this offset include major element chemistry differences between natural and experimental samples or differences in the pressures and temperatures that natural vs. experimental samples experienced (e.g., Warren and Hauri 2014).

The data set for fluorine partitioning between orthopyroxene and clinopyroxene is much smaller than that for water. A literature compilation of natural samples (Gazel et al. 2012; Warren and Hauri 2014) combined with our data set yields a partition coefficient of 3.0 ± 1.0 (Fig. 7b). Similar to water, the partition coefficient determined by experiments (Dalou et al. 2012; Rosenthal et al. 2015) is smaller than that seen in natural samples, averaging $D_F^{Cpx/Opx} = 1.5 \pm 0.6$.

The phosphorus data set for natural mantle samples in the literature is also limited and shows a larger amount of scatter than fluorine (Fig. 7c). The combination of our data with other studies measuring phosphorus in natural mantle samples (Witt-Eickschen and O'Neill 2005; Mallmann et al. 2009; Gazel et al. 2012; Warren and Hauri 2014) results in a partition coefficient of 2.7 ± 1.3. Possible reasons for the scatter in this data set, and thus the high uncertainty in this partition coefficient, include a change in substitution mechanism, as suggested by Witt-Eickschen and O'Neill (2005) and supported by Mallmann et al. (2009), zoning in phosphorus content as suggested by the data presented here, or disequilibrium in phosphorus content due to diffusion. We do not know of any experimental partition coefficients for phosphorus between orthopyroxene and clinopyroxene.

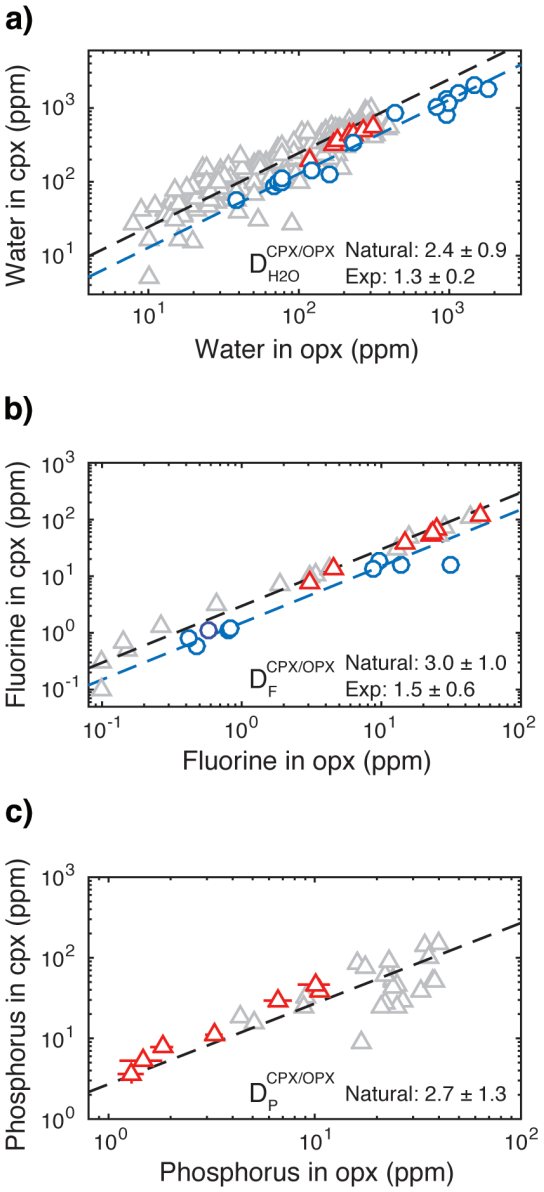

Figure 7. Partitioning behavior between orthopyroxene and clinopyroxene for water (**a**), fluorine (**b**), and phosphorus (**c**). For all plots, data from this study are red triangles, data from previous studies on natural samples are gray triangles, and experimental data are blue circles. The partition coefficient for all natural samples, including those from this study, is shown as a black dashed line, while the experimental partition coefficient is shown as a blue dashed line. 1σ uncertainties in the volatile content for data from this study are shown unless smaller than the symbol. Uncertainties in the partition coefficients are 1σ. See text for references.

Implications

We have produced a set of natural reference materials for measuring volatiles, particularly water, in mantle minerals via SIMS to facilitate the use of this technique at more laboratories around the world. We have created a calibration mount of previously analyzed grains of orthopyroxene and clinopyroxene, along with a set of basaltic glasses and a Suprasil 3002 glass blank.

This calibration mount is available for use in cross-calibrating new grains of these reference materials against the specific grains measured in this study. Sample material is available by request to the Department of Mineral Sciences at the Museum of Natural History, Smithsonian Institution. New grains from these samples should plot within the currently measured water concentration ranges of these samples. However, because intergranular variations are always possible, future grains from these samples should be calibrated against the grains measured in this study.

The fluorine and phosphorus contents of the reference materials in this study have also been measured, and fluorine in particular is quite homogeneous. These reference materials can be used to create calibrations for low concentrations of both fluorine and phosphorus, though these calibrations will be no better than ones created using basaltic glass as they are based on glasses. More work must be done to resolve potential matrix effects for these elements, both between glasses with different silica contents and between glass and pyroxene.

Acknowledgments

We thank Jason Harvey, Anne Peslier, and Alan Brandon for donating samples for analysis; the Department of Mineral Sciences, Smithsonian Institution, for loaning sample material and Leslie Hale for assisting with access to that material; and Chuck Hitzman for assistance with the NanoSIMS at Stanford. We also thank reviewers Anne Peslier and Jed Mosenfelder and Associate Editor Roland Stalder for their thoughtful comments. This material is based upon work supported by the National Science Foundation under Grant No. EAR-1255620 to J.M.W. and Grant No. EAR-1524581 to E.H.H., and by the Stanford Nano Shared Facilities through a seed grant to J.M.W.

References cited

Aubaud, C., Hauri, E.H., and Hirschmann, M.M. (2004) Hydrogen partition coefficients between nominally anhydrous minerals and basaltic melts. Geophysical Research Letters, 31, L20611.

Aubaud, C., Withers, A.C., Hirschmann, M.M., Guan, Y., Leshin, L.A., Mackwell, S.J., and Bell, D.R. (2007) Intercalibration of FTIR and SIMS for hydrogen measurements in glasses and nominally anhydrous minerals. American Mineralogist, 92, 811–828.

Aubaud, C., Bureau, H., Raepsaet, C., Khodja, H., Withers, A.C., Hirschmann, M.M., and Bell, D.R. (2009) Calibration of the infrared molar absorption coefficients for H in olivine, clinopyroxene and rhyolitic glass by elastic recoil detection analysis. Chemical Geology, 262, 78–86.

Bell, D.R., and Rossman, G.R. (1992) Water in Earth's mantle: The role of nominally anhydrous minerals. Science, 255, 1391–1397.

Bell, D.R., Ihinger, P.D., and Rossman, G.R. (1995) Quantitative analysis of trace OH in garnet and pyroxenes. American Mineralogist, 80, 465–474.

Bell, D.R., Rossman, G.R., Maldener, J., Endisch, D., and Rauch, F. (2003) Hydroxide in olivine: A quantitative determination of the absolute amount and calibration of the IR spectrum. Journal of Geophysical Research, 108, 2105.

Bell, D.R., Rossman, G.R., and Moore, R.O. (2004) Abundance and partitioning of OH in a high-pressure magmatic system: Megacrysts from the Monastery Kimberlite, South Africa. Journal of Petrology, 45, 1539–1564.

Bizimis, M., and Peslier, A.H. (2015) Water in Hawaiian garnet pyroxenites: Implications for water heterogeneity in the mantle. Chemical Geology, 397, 61–75.

Bonadiman, C., Hao, Y., Coltorti, M., Dallai, L., Faccini, B., Huang, Y., and Xia, Q. (2009) Water contents of pyroxenes in intraplate lithospheric mantle. European Journal of Mineralogy, 21, 637–647.

Brandon, A.D., and Draper, D.S. (1996) Constraints on the origin of the oxidation state of mantle overlying subduction zones: An example from Simcoe, Washington, USA. Geochimica et Cosmochimica Acta, 60, 1739–1749.

Brunet, F., and Chazot, G. (2001) Partitioning of phosphorus between olivine, clinopyroxene and silicate glass in a spinel lherzolite xenolith from Yemen. Chemical Geology, 176, 51–72.

Bryan, W.B., and Moore, J.G. (1977) Compositional variations of young basalts in the Mid-Atlantic Ridge rift valley near lat 36°49′N. Geological Society of America Bulletin, 88, 556–570.

Dalou, C., Koga, K.T., Shimizu, N., Boulon, J., and Devidal, J.-L. (2012) Experimental determination of F and Cl partitioning between lherzolite and basaltic melt. Contributions to Mineralogy and Petrology, 163, 591–609.

Deline, V.R., Katz, W., Evans, C.A. Jr., and Williams, P. (1978) Mechanism of the SIMS matrix effect. Applied Physics Letters, 33, 832–835.

Demouchy, S., Jacobsen, S.D., Gaillard, F., and Stern, C.R. (2006) Rapid magma ascent recorded by water diffusion profiles in mantle olivine. Geology, 34, 429.

Denis, C.M.M., Demouchy, S., and Shaw, C.S.J. (2013) Evidence of dehydration in peridotites from Eifel Volcanic Field and estimates of the rate of magma ascent. Journal of Volcanology and Geothermal Research, 258, 85–99.

Doucet, L.S., Peslier, A.H., Ionov, D.A., Brandon, A.D., Golovin, A.V., Goncharov, A.G., and Ashchepkov, I.V. (2014) High water contents in the Siberian cratonic mantle linked to metasomatism: An FTIR study of Udachnaya peridotite xenoliths. Geochimica et Cosmochimica Acta, 137, 159–187.

Endisch, D., Sturm, H., and Rauch, F. (1994) Nuclear reaction analysis of hydrogen at levels below 10 at.ppm. Nuclear Instruments and Methods in Physics Research B, 84, 380–392.

Falus, G., Tommasi, A., Ingrin, J., and Szabó, C. (2008) Deformation and seismic anisotropy of the lithospheric mantle in the southeastern Carpathians inferred from the study of mantle xenoliths. Earth and Planetary Science Letters, 272, 50–64.

Gazel, E., Plank, T., Forsyth, D.W., Bendersky, C., Lee, C.-T.A., and Hauri, E.H. (2012) Lithosphere versus asthenosphere mantle sources at the Big Pine Volcanic Field, California. Geochemistry, Geophysics, Geosystems, 13, 1–25.

Goldman, D.S., and Rossman, G.R. (1976) Identification of a mid-infrared electronic absorption band of Fe^{2+} in the distorted M(2) site of Orthopyroxene, (Mg, Fe)SiO_3. Chemical Physics Letters, 41, 474–475.

Grant, K., Ingrin, J., Lorand, J.P., and Dumas, P. (2007) Water partitioning between mantle minerals from peridotite xenoliths. Contributions to Mineralogy and Petrology, 154, 15–34.

Hao, Y., Xia, Q., Liu, S., Feng, M., and Zhang, Y. (2012) Recognizing juvenile and relict lithospheric mantle beneath the North China Craton: Combined analysis of H_2O, major and trace elements and Sr-Nd isotope compositions of clinopyroxenes. Lithos, 149, 136–145.

Hao, Y., Xia, Q., Li, Q., Chen, H., and Feng, M. (2014) Partial melting control of water contents in the Cenozoic lithospheric mantle of the Cathaysia block of South China. Chemical Geology, 380, 7–19.

Hao, Y.-T., Xia, Q.-K., Jia, Z.-B., Zhao, Q.-C., Li, P., Feng, M., and Liu, S.-C. (2016) Regional heterogeneity in the water content of the Cenozoic lithospheric mantle of Eastern China. Journal of Geophysical Research: Solid Earth, 121, 1–21.

Harvey, J., Yoshikawa, M., Hammond, S.J., and Burton, K.W. (2012) Deciphering the trace element characteristics in Kilbourne Hole peridotite xenoliths: Melt-rock interaction and metasomatism beneath the Rio Grande Rift, SW USA. Journal of Petrology, 53, 1709–1742.

Hauri, E., Wang, J., Dixon, J.E., King, P.L., Mandeville, C., and Newman, S. (2002) SIMS analysis of volatiles in silicate glasses 1. Calibration, matrix effects and comparisons with FTIR. Chemical Geology, 183, 99–114.

Hauri, E.H., Shaw, A.M., Wang, J., Dixon, J.E., King, P.L., and Mandeville, C. (2006) Matrix effects in hydrogen isotope analysis of silicate glasses by SIMS. Chemical Geology, 235, 352–365.

Hawkins, J.W., Lonsdale, P.F., Macdougall, J.D., and Volpe, A.M. (1990) Petrology of the axial ridge of the Mariana Trough backarc spreading center. Earth and Planetary Science Letters, 100, 226–250.

Hirschmann, M.M. (2006) Water, melting, and the deep earth H_2O cycle. Annual Review of Earth and Planetary Sciences, 34, 629–653.

Hirth, G., and Kohlstedt, D.L. (1996) Water in the oceanic upper mantle: implications for rheology, melt extraction and the evolution of the lithosphere. Earth and Planetary Science Letters, 144, 93–108.

Hui, H., Peslier, A.H., Rudnick, R.L., Simonetti, A., and Neal, C.R. (2015) Plume-cratonic lithosphere interaction recorded by water and other trace elements in peridotite xenoliths from the Labait volcano, Tanzania. Geochemistry, Geophysics, Geosystems, 16, 1–24.

Karato, S. (1990) The role of hydrogen in the electrical conductivity of the upper mantle. Nature, 347, 272–273.

Karato, S.-i., Paterson, M.S., and Fitzgerald, J.D. (1986) Rheology of synthetic olivine aggregates: influence of grain size and water. Journal of Geophysical Research, 91, 8151–8176.

Katayama, I., Jung, H., and Karato, S.-i. (2004) New type of olivine fabric from deformation experiments at modest water content and low stress. Geology, 32, 1045.

Koga, K., Hauri, E., Hirschmann, M., and Bell, D. (2003) Hydrogen concentration analyses using SIMS and FTIR: Comparison and calibration for nominally anhydrous minerals. Geochemistry, Geophysics, Geosystems, 4.

Kovács, I., O'Neill, H.St.C., Hermann, J., and Hauri, E.H. (2010) Site-specific infrared O-H absorption coefficients for water substitution into olivine. American Mineralogist, 95, 292–299.

Kushiro, I., Syono, Y., and Akimoto, S.-i. (1968) Melting of a peridotite nodule at high pressures and high water pressures. Journal of Geophysical Research, 73, 6023–6029.

Le Voyer, M., Cottrell, E., Kelley, K.A., Brounce, M., and Hauri, E.H. (2015) The effect of primary versus secondary processes on the volatile content of MORB glasses: An example from the equatorial Mid-Atlantic Ridge (5°N-2°S). Journal of Geophysical Research: Solid Earth, 120, 125–144.

Li, Z.-X.A., Lee, C.-T.A., Peslier, A.H., Lenardic, A., and Mackwell, S.J. (2008)

Water contents in mantle xenoliths from the Colorado Plateau and vicinity: Implications for the mantle rheology and hydration-induced thinning of continental lithosphere. Journal of Geophysical Research: Solid Earth, 113, B09210.
Libowitzky, E., and Rossman, G.R. (1996) Principles of quantitative absorbance measurements in anisotropic crystals. Physics and Chemistry of Minerals, 23, 319–327.
——— (1997) An IR absorption calibration for water in minerals. American Mineralogist, 82, 1111–1115.
Ludwig, T., and Stalder, R. (2007) A new method to eliminate the influence of in situ contamination in SIMS analysis of hydrogen. Journal of Analytical Atomic Spectrometry, 22, 1415–1419.
Luhr, J.F., and Aranda-Gomez, J.J. (1997) Mexican peridotite xenoliths and tectonic terranes: Correlations among vent location, texture, temperature, pressure, and oxygen fugacity. Journal of Petrology, 38, 1075–1112.
Mackwell, S.J., Kohlstedt, D.L., and Paterson, M.S. (1985) The role of water in the deformation of olivine single crytals. Journal of Geophysical Research, 90, 11,319–11,333.
Maldener, J., Hösch, A., Langer, K., and Rauch, F. (2003) Hydrogen in some natural garnets studied by nuclear reaction analysis and vibrational spectroscopy. Physics and Chemistry of Minerals, 30, 337–344.
Mallmann, G., O'Neill, H.St.C., and Klemme, S. (2009) Heterogeneous distribution of phosphorus in olivine from otherwise well-equilibrated spinel peridotite xenoliths and its implications for the mantle geochemistry of lithium. Contributions to Mineralogy and Petrology, 158, 485–504.
Mei, S., and Kohlstedt, D.L. (2000) Influence of water on plastic deformation of olivine aggregates 2. Dislocation creep regime. Journal of Geophysical Research, 105, 21471–21481.
Milman-Barris, M.S., Beckett, J.R., Baker, M.B., Hofmann, A.E., Morgan, Z., Crowley, M.R., Vielzeuf, D., and Stolper, E. (2008) Zoning of phosphorus in igneous olivine. Contributions to Mineralogy and Petrology, 155, 739–765.
Mosenfelder, J.L., and Rossman, G.R. (2013a) Analysis of hydrogen and fluorine in pyroxenes: I. Orthopyroxene. American Mineralogist, 98, 1026–1041.
——— (2013b) Analysis of hydrogen and fluorine in pyroxenes: II. Clinopyroxene. American Mineralogist, 98, 1042–1054.
Mosenfelder, J.L., Le Voyer, M., Rossman, G.R., Guan, Y., Bell, D.R., Asimow, P.D., and Eiler, J.M. (2011) Analysis of hydrogen in olivine by SIMS: Evaluation of standards and protocol. American Mineralogist, 96, 1725–1741.
Paterson, M.S. (1982) The determination of hydroxyl by infrared absorption in quartz, silicate glasses, and similar materials. Bulletin of Mineralogy, 105, 20–29.
Peslier, A.H. (2010) A review of water contents of nominally anhydrous natural minerals in the mantles of Earth, Mars and the Moon. Journal of Volcanology and Geothermal Research, 197, 239–258.
Peslier, A.H., and Bizimis, M. (2015) Water in Hawaiian peridotite minerals: A case for a dry metasomatized oceanic mantle lithosphere. Geochemistry, Geophysics, Geosystems, 16, 1211–1232.
Peslier, A.H., Luhr, J.F., and Post, J. (2002) Low water contents in pyroxenes from spinel-peridotites of the oxidized, sub-arc mantle wedge. Earth and Planetary Science Letters, 201, 69–86.
Peslier, A.H., Woodland, A.B., Bell, D.R., Lasarov, M., and Lapen, T.J. (2012) Metasomatic control of water contents in the Kaapvaal cratonic mantle. Geochimica et Cosmochimica Acta, 97, 213–246.
Rooks, E., Gibson, S., Leat, P., and Petrone, C.M. (2015) Compositionally controlled volatile content of nominally volatile-free minerals in the continental upper mantle of southern Gondwana (Patagonia & W. Antarctica). American Geophysical Union Fall Meeting, San Francisco, Abstract V51I-02.
Rosenthal, A., Hauri, E.H., and Hirschmann, M.M. (2015) Experimental determination of C, F, and H partitioning between mantle minerals and carbonated basalt, CO_2/Ba and CO_2/Nb systematics of partial melting, and the CO_2 contents of basaltic source regions. Earth and Planetary Science Letters, 412, 77–87.
Rossman, G. (2006) Analytical methods for measuring water in nominally anhydrous minerals. Reviews in Mineralogy and Geochemistry, 62, 1–28.
Sarafian, E., Evans, R.L., Collins, J.A., Elsenbeck, J., Gaetani, G.A., Gaherty, J.B., Hirth, G., and Lizarralde, D. (2015) The electrical structure of the central Pacific upper mantle constrained by the NoMelt experiment. Geochemistry, Geophysics, Geosystems, 16, 1115–1132.
Schlechter, E., Stalder, R., and Behrens, H. (2012) Electrical conductivity of H-bearing orthopyroxene single crystals measured with impedance spectroscopy. Physics and Chemistry of Minerals, 39, 531–541.
Smyth, J.R., Bell, D.R., and Rossman, G.R. (1991) Incorporation of hydroxyl in upper-mantle clinopyroxenes. Nature, 351, 732–735.
Stalder, R., Klemme, S., Ludwig, T., and Skogby, H. (2005) Hydrogen incorporation in orthopyroxene: interaction of different trivalent cations. Contributions to Mineralogy and Petrology, 150, 473–485.
Stalder, R., Prechtel, F., and Ludwig, T. (2012) No site-specific infrared absorption coefficients for OH-defects in pure enstatite. European Journal of Mineralogy, 24, 465–470.
Stolper, E., and Newman, S. (1994) The role of water in the petrogenesis of Mariana trough magmas. Earth and Planetary Science Letters, 121, 293–325.
Tarassoff, P., and Gault, R.A. (1994) The Orford Nickel Mine, Quebec, Canada. Mineralogical Record, 25, 327–345.
Tenner, T.J., Hirschmann, M.M., Withers, A.C., and Hervig, R.L. (2009) Hydrogen partitioning between nominally anhydrous upper mantle minerals and melt between 3 and 5 GPa and applications to hydrous peridotite partial melting. Chemical Geology, 262, 42–56.
Toplis, M.J., Libourel, G., and Carroll, M.R. (1994) The role of phosphorus in crystallisation processes of basalt: An experimental study. Geochimica et Cosmochimica Acta, 58, 797–810.
Turner, M., Ireland, T., Hermann, J., Holden, P., Padrón-Navarta, J.A., Hauri, E.H., and Turner, S. (2015) Sensitive high resolution ion microprobe–stable isotope (SHRIMP-SI) analysis of water in silicate glasses and nominally anhydrous reference minerals. Journal of Analytical Atomic Spectrometry, 30, 1706–1722.
Volpe, A.M., Macdougall, J.D., Lugmair, G.W., Hawkins, J.W., and Lonsdale, P. (1990) Fine-scale isotopic variation in Mariana Trough basalts: evidence for heterogeneity and a recycled component in backarc basin mantle. Earth and Planetary Science Letters, 100, 251–264.
Warren, J.M. (2016) Global variations in abyssal peridotite compositions. Lithos, 248-251, 193–219.
Warren, J.M., and Hauri, E.H. (2014) Pyroxenes as tracers of mantle water variations. Journal of Geophysical Research: Solid Earth, 119, 1851–1881.
Watson, E.B., Cherniak, D.J., and Holycross, M.E. (2015) Diffusion of phosphorus in olivine and molten basalt. American Mineralogist, 100, 2053–2065.
Welsch, B., Hammer, J., and Hellebrand, E. (2014) Phosphorus zoning reveals dendritic architecture of olivine. Geology, 42, 867–870.
Withers, A.C., Hirschmann, M.M., and Tenner, T.J. (2011) The effect of Fe on olivine H_2O storage capacity: Consequences for H_2O in the martian mantle. American Mineralogist, 96, 1039–1053.
Withers, A.C., Bureau, H., Raepsaet, C., and Hirschmann, M.M. (2012) Calibration of infrared spectroscopy by elastic recoil detection analysis of H in synthetic olivine. Chemical Geology, 334, 92–98.
Witt-Eickschen, G., and O'Neill, H.St.C. (2005) The effect of temperature on the equilibrium distribution of trace elements between clinopyroxene, orthopyroxene, olivine and spinel in upper mantle peridotite. Chemical Geology, 221, 65–101.
Wright, K., and Catlow, C.R.A. (1994) A computer simulation study of (OH) defects in olivine. Physics and Chemistry of Minerals, 20, 515–518.
Xia, Q.-K., Hao, Y., Li, P., Deloule, E., Coltorti, M., Dallai, L., Yang, X., and Feng, M. (2010) Low water content of the Cenozoic lithospheric mantle beneath the eastern part of the North China Craton. Journal of Geophysical Research, 115, B07207.
Xia, Q.-K., Hao, Y.-T., Liu, S.-C., Gu, X.-Y., and Feng, M. (2013) Water contents of the Cenozoic lithospheric mantle beneath the western part of the North China Craton: Peridotite xenolith constraints. Gondwana Research, 23, 108–118.
Yang, X.-Z., Xia, Q.-K., Deloule, E., Dallai, L., Fan, Q.-C., and Feng, M. (2008) Water in minerals of the continental lithospheric mantle and overlying lower crust: A comparative study of peridotite and granulite xenoliths from the North China Craton. Chemical Geology, 256, 33–45.
Yu, Y., Xu, X.-S., Griffin, W.L., O'Reilly, S.Y., and Xia, Q.-K. (2011) H_2O contents and their modification in the Cenozoic subcontinental lithospheric mantle beneath the Cathaysia block, SE China. Lithos, 126, 182–197.

Manuscript received May 23, 2016
Manuscript accepted October 4, 2016
Manuscript handled by Roland Stalder